

Outcome Correlation in Graph Neural Network Regression

Junteng Jia
Cornell University
jj585@cornell.edu

Austin R. Benson
Cornell University
arb@cs.cornell.edu

ABSTRACT

Graph neural networks aggregate features in vertex neighborhoods to learn vector representations of all vertices, using supervision from some labeled vertices during training. The predictor is then a function of the vector representation, and predictions are made independently on unlabeled nodes. This widely-adopted approach implicitly assumes that vertex labels are independent after conditioning on their neighborhoods. We show that this strong assumption is far from true on many real-world graph datasets and severely limits predictive power on a number of regression tasks. Given that traditional graph-based semi-supervised learning methods operate in the opposite manner by explicitly modeling the correlation in predicted outcomes, this limitation may not be all that surprising.

Here, we address this issue with a simple and interpretable framework that can improve any graph neural network architecture by modeling correlation structure in regression outcome residuals. Specifically, we model the joint distribution of outcome residuals on vertices with a parameterized multivariate Gaussian, where the parameters are estimated by maximizing the marginal likelihood of the observed labels. Our model achieves substantially boosts the performance of graph neural networks, and the learned parameters can also be interpreted as the strength of correlation among connected vertices. To allow us to scale to large networks, we design linear time algorithms for low-variance, unbiased model parameter estimates based on stochastic trace estimation. We also provide a simplified version of our method that makes stronger assumptions on correlation structure but is extremely easy to implement and provides great practical performance in several cases.

1 INTRODUCTION

Graphs are standard representations for wide-ranging complex systems with interacting entities, such as social networks, election maps, and transportation systems [8, 9, 23]. Typically, a graph represents entities as vertices (nodes) and the interactions as edges that connect two vertices. In many cases, the vertices also have several attributes; for example, an online social network may have information on a person’s location, gender, and interests. Semi-supervised prediction problems on graphs combine the graph topology and vertex attributes with some labels on a subset of vertices to make predictions for vertices where such labels are missing. Continuing our online social network example, we may have the age of some users from registration or survey data and want to infer the age of other users for better targeted advertising. Or, in U.S. election map networks, we may have polling data from some counties and wish to predict outcomes in other ones, given commonly available demographic features for all the counties.

These problems fall under the umbrella of semi-supervised learning for graph-structured data. Graph neural networks (GNNs) are a class of methods that have had great success on such tasks [14, 21, 31, 39], largely due to their ability to extract information from

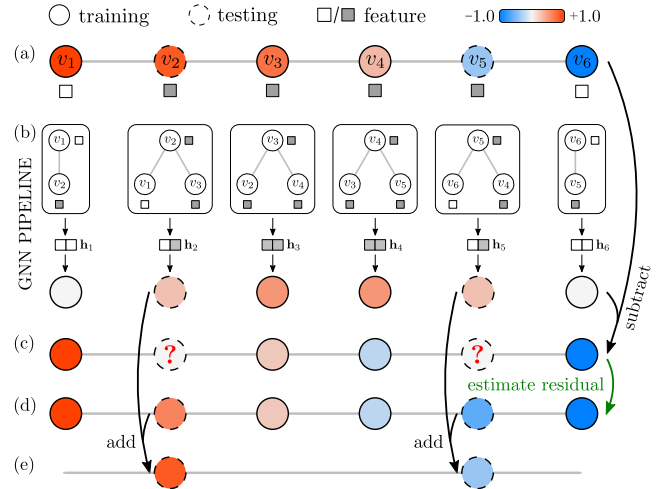


Figure 1: Limitations of GNN regression and our proposed fix. The vertex labels decrease from v_1 (+1.0) to v_6 (-1.0), and most interior vertices have positive-valued labels. (a) Each vertex’s degree is used as its feature, and vertices are colored based on their labels. The training vertices are v_1, v_3, v_4, v_6 . (b) The GNN encodes vertex neighborhoods by vectors h_i , which are used independently for label prediction. The GNN captures the positive trend for interior vertices but fails to distinguish v_1, v_2, v_3 from v_6, v_5, v_4 due to graph symmetry. (c) GNN regression residuals for the training vertices. (d) Our *Correlated GNN* method estimates the residuals on testing vertices v_2, v_5 . (e) The estimated residuals are added to GNN outputs as our final predictions, yielding good estimates.

vertex features. Their popularity has also been boosted by their scalability and inductive learning capabilities [4, 30, 36]. The basic idea of GNNs is to first encode the local environment of each vertex into a vector representation, by transforming and aggregating its own features along with the features of its neighbors in the graph [15] and then predict the label of each vertex with its vector representation. Many target applications are for classification.¹ We instead focus on regression problems for fine-grained prediction; for example, in our U.S. election example above, a candidate would like to predict their vote share in each county to plan a campaign strategy. At a first glance, existing GNN architectures can easily be adapted for regression problems by simply changing the output layer and choosing a loss function such as the squared error in the predicted value; automatic differentiation handles the rest.

However, a fundamental limitation of GNNs is that they predict each vertex label independently given its vertex representation and ignore label correlation of neighboring vertices. Specifically, a prediction depends on the model parameters, the features of a vertex

¹Perhaps the most well-studied problem in this space is predicting the “type” of an academic paper in a citation network.

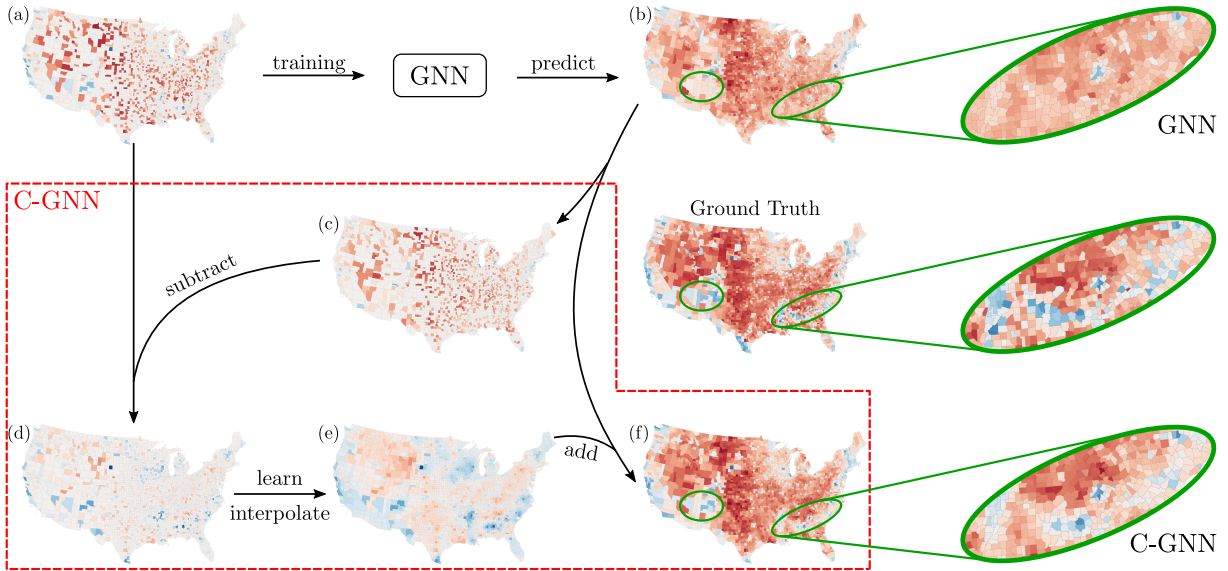


Figure 2: Our Correlated GNN (C-GNN) framework for predicting county-level outcomes in the 2016 U.S. presidential election. (a) The inputs are the county adjacency matrix, county-level demographic features, and 30% of the labels. (b) The GNN makes base predictions. (c–d) The GNN predictions on the training data (c) show that the regression residual (d) is correlated amongst neighboring counties. (e) Our C-GNN model learns the residual correlation and interpolates to get the residual on testing counties. (f) Adding predicted residuals on the test counties to the GNN base prediction substantially increases accuracy.

and other vertices in its neighborhood but *not* on the predictions of neighboring vertices. While not stated in these terms, similar observations have been made about such limitations [24, 34, 37]. Figures 1a and 1b show an example illustrating why this is problematic, using a graph with topological and feature symmetry but monotonically varying vertex labels. In this example, a GNN fails to distinguish vertex v_2 from v_4 and therefore cannot predict correct labels for both of them. On the other hand, traditional graph-based semi-supervised learning algorithms (e.g., those based on label propagation [38, 40]), work very well in this case as the labels vary smoothly over the graph. Of course, in many applications, vertex features are remarkably informative. Still, gains in performance on benchmark tasks from using vertex features have in some sense put blinders on the modeler — the methodological focus is on squeezing more and more information from the features [39], ignoring signal in the joint distribution of the outcome.

In Fig. 1, vertex features partially explain the outcomes. The features are somewhat — but not overwhelmingly — predictive. The question then arises: when features are only somewhat predictive, can we also directly take advantage of outcome correlations? Or, put another way, can we get bigger gains in predictive power by exploiting outcome correlations, rather than squeezing minuscule additional signal in features with more complicated architectures?

The present work: Correlated Graph Neural Networks. To answer the above questions in the affirmative, we propose *Correlated Graph Neural Networks* (C-GNNs). The basic idea of C-GNNs is to use a GNN as a base regressor to capture the (possibly mild) outcome dependency on vertex features and then further model the regression residuals on all vertices (Figs. 1c to 1e). While one

can model the residual in many ways, we use a simple multivariate Gaussian with a sparse precision matrix based on the graph topology. We learn the correlation structure by maximizing the marginal likelihood of the training vertex labels. At inference time, our model then predicts the outcomes on testing vertices by maximizing their probability conditioned on the training labels. Importantly, our method covers the original GNN as a special case: minimizing squared-error loss with respect to the GNN is the maximum likelihood estimator when the precision matrix is the identity (errors are uncorrelated). We also make no assumption on the GNN architecture, as our methodology “sits on top” of the base regressor.

For a real-world data example, we predict the county-level margin of victory in the 2016 U.S. presidential election (Fig. 2). Each county is represented by a vertex with demographic features such as migration rate, education level, and median household income; edges connect bordering counties. While the GNN captures correlation between vertex features and outcomes (Figs. 2a and 2b), our C-GNN leverages residual correlation (Figs. 2c to 2f) to boost test R^2 from 0.45 to 0.63. The green circles show regions where the GNN produces large errors that are corrected by C-GNN.

More generally, we can replace the GNN base regressor with any feature-based predictor, e.g., a linear model or multilayer perceptron, and our regression pipeline is unchanged. With a linear model, for example, our framework is essentially performing generalized least squares [27], where the precision matrix structure is given by the graph. In practice, we find that within our framework, a GNN base regressor indeed works well for graph-structured data.

Our C-GNN consistently outperforms the base GNN and other competing baselines by large margins: C-GNNs achieves a mean 14% improvement in R^2 over GNNs for our datasets. Furthermore, using a simple multilayer perceptron (that does not use neighborhood

features) as the base regressor, our framework even outperforms a standard GNN in most experiments. This highlights the importance of outcome correlation and suggests that focusing on minor GNN architecture improvements may not always be the right strategy.

Thus far, we have considered transductive learning, but another standard setup for machine learning on graphs is *inductive learning*: a model is trained on one graph where labels are widely available and deployed on other graphs where labels are more difficult to obtain. Assuming that the learned GNN and the residual correlation generalize to unseen graphs, our framework can simply condition on labeled vertices (if available) in a new graph to improve regression accuracy. Indeed, these assumptions hold for many real-world datasets that we consider. With a small fraction of labels in the new graphs, inductive accuracies of our C-GNN are even better than transductive accuracies of a GNN. For example, we train a model to predict county-level unemployment rates using 60% of labeled vertices in 2012. Given 10% of labels in the 2016 data, C-GNN achieves 0.65 test R^2 on unlabeled vertices, which is even more accurate than GNN trained directly on 60% of 2016 labels ($R^2 = 0.53$).

We also develop efficient numerical techniques that make model optimization tractable. Standard factorization-based algorithms for the log marginal likelihood and derivatives computation takes $\mathcal{O}(n^3)$ operations, where n is the number of nodes; such approaches do not scale beyond graphs with a few thousand vertices. To remedy this, we use stochastic estimation [13, 29] to take full advantage of our sparse and well-conditioned precision matrix, which reduces the computational scaling to $\mathcal{O}(m)$, where m is the number of edges, producing low-variance unbiased parameter estimates. We further introduce a simplified version of our method that assumes positive correlation among neighboring residuals, which is common in real-world data. The algorithm is extremely simple: train a standard GNN and then run label propagation to interpolate GNN residuals on the testing vertices. We call this LP-GNN and find that it also outperforms standard GNNs by a wide margin on most datasets.

2 METHODOLOGY

Let $G = (V, E, \{\mathbf{x}_i\})$ be a graph, where V is the vertex set ($n = |V|$), E is the edge set ($m = |E|$), and \mathbf{x}_i denotes the features for vertex $i \in V$. We consider the semi-supervised vertex label regression problem: given real-valued labels² y_L on a subset of vertices $L \subseteq V$, predict labels on the rest of vertices $U \equiv V \setminus L$. In this section, we first review GNNs and discuss its implicit statistical assumptions. As our experiments in Section 4 show, these assumption are often invalid in real-world graph data. Motivated by this insight, we improve the predictive power of GNNs by explicitly modeling label correlations with a multivariate Gaussian distribution, and introduce efficient numerical techniques for model inference.

2.1 Statistical Interpretation of Standard GNNs

In a standard GNN regression pipeline, the features in the neighborhood of a vertex get encoded into a vertex representation,³ and each

²The terms “labels”, “outcomes”, and “targets” are used interchangeably in this paper.

³For instance, a K -step graph convolution network (GCN) computes vertex representations by repeated local feature averaging, transformation, and nonlinear activation:

$$\mathbf{h}_i^{(0)} = \mathbf{x}_i; \quad \mathbf{h}_i^{(k)} = \phi \left(\mathbf{W}^{(k)} \cdot \text{MEAN} \left(\{\mathbf{h}_i^{(k-1)}\} \cup \{\mathbf{h}_j^{(k-1)} : j \in N_i(i)\} \right) \right); \quad \mathbf{h}_i = \mathbf{h}_i^{(K)}$$

, where $\mathbf{W}^{(k)}$ is weight matrix at step- k , and ϕ is a non-linear activation function.

vertex representation is used independently for label prediction:

$$\mathbf{h}_i = f(\mathbf{x}_i, \{\mathbf{x}_j : j \in N_K(i)\}, \theta); \quad \hat{y}_i = g(\mathbf{h}_i, \theta). \quad (1)$$

Here, $N_K(i)$ denotes the K -hop neighborhood of vertex i . Oftentimes, $K = 2$ [14, 21]. The GNN weights θ are trained using observed labels, and the most common loss for regression is the squares loss:

$$\sum_{i \in L} (g(\mathbf{h}_i, \theta) - y_i)^2. \quad (2)$$

Following standard statistical arguments common for ordinary least squares [11], minimizing the loss in Eq. (2) in our setup is equivalent to maximizing the likelihood of a fully factorizable joint distribution of labels, where each label distribution conditioned on the vertex representation is a univariate Gaussian:

$$p(\mathbf{y} | G) = \prod_{i \in V} p(y_i | \mathbf{h}_i); \quad y_i | \mathbf{h}_i \sim \mathcal{N}(\hat{y}_i, \sigma^2) \quad (3)$$

Consequently, the errors in the estimates $y_i - \hat{y}_i$ are independent with mean zero. There’s no reason to assume independence, and in cases such as election data, accounting for error correlation is critical.⁴ We thus consider correlation structure next.

2.2 Correlation as a Multivariate Gaussian

We now propose a model that can exploit label correlation. Specifically, we model the joint distribution of vertex labels with a multivariate Gaussian:

$$\mathbf{y} \sim \mathcal{N}(\hat{\mathbf{y}}, \Gamma^{-1}) \quad \text{or equivalently, } \mathbf{r} \equiv \mathbf{y} - \hat{\mathbf{y}} \sim \mathcal{N}(\mathbf{0}, \Gamma^{-1}), \quad (4)$$

where $\Gamma = \Sigma^{-1}$ is the inverse covariance (or precision) matrix, and \mathbf{r} is the residual of GNN regression. Here, we parameterize the precision matrix in a way that (i) uses the graph topology and (ii) will be computationally tractable:

$$\Gamma = \beta(\mathbf{I} - \alpha\mathbf{S}), \quad (5)$$

where \mathbf{I} is the identity matrix and $\mathbf{S} = \mathbf{D}^{-1/2}\mathbf{A}\mathbf{D}^{-1/2}$ is the normalized adjacency matrix. The scalar β controls the overall magnitude of the residual, and the scalar α reflects the correlation structure. The sign of α measures the direction of correlation (positive or negative), and the magnitude measures the strength of correlation.

Validity of the multivariate Gaussian requires that Γ is positive definite. This requirement is easily satisfied by restricting $-1 < \alpha < 1$ and $\beta > 0$. First, we verify both $(\mathbf{I} + \mathbf{S})$ and $(\mathbf{I} - \mathbf{S})$ are positive semi-definite by expanding their quadratic form with any $\mathbf{z} \in \mathbb{R}^n$:

$$\begin{aligned} \mathbf{z}^\top (\mathbf{I} + \mathbf{S}) \mathbf{z} &= \sum_{(i,j) \in E} (z_i/\sqrt{D_{ii}} + z_j/\sqrt{D_{jj}})^2 \geq 0 \\ \mathbf{z}^\top (\mathbf{I} - \mathbf{S}) \mathbf{z} &= \sum_{(i,j) \in E} (z_i/\sqrt{D_{ii}} - z_j/\sqrt{D_{jj}})^2 \geq 0 \end{aligned} \quad (6)$$

For $0 \leq \alpha < 1$, $\Gamma = (1 - \alpha)\beta\mathbf{I} + \alpha\beta(\mathbf{I} - \mathbf{S}) > 0$ since the first term is strictly positive definite, and the second term is positive semi-definite. A similarly argument holds for $-1 < \alpha < 0$. Two special cases of the precision matrix in Eq. (5) deserve special attention. First, when $\alpha = 0$, Γ is the identity matrix (up to constant scaling), and the model reduces to the standard GNN regression. Second, in the limit $\alpha \rightarrow 1$, Γ is the normalized Laplacian matrix, and the noise is assumed to be smooth over the entire graph. The normalized Laplacian matrix is only positive semi-definite, therefore we make

⁴<https://fivethirtyeight.com/features/a-users-guide-to-fivethirtyeight-2016-general-election-forecast/>

Algorithm 1: C-GNN label inference.

Input : normalized adjacency matrix S ; features $\{\mathbf{x}_i\}$;
training labels \mathbf{y}_L ; parameters α, β ; GNN weights θ
Output: predicted labels $\mathbf{y}_U^{\text{C-GNN}}$ for unknown vertices

```

1  $\Gamma \leftarrow \beta(\mathbf{I} - \alpha S)$  ▷ precision matrix
2  $\mathbf{h}_i \leftarrow f(\mathbf{x}_i, \{\mathbf{x}_j : j \in N_K(i)\}, \theta), \forall i \in V$  ▷ GNN learning
3  $\hat{\mathbf{y}}_i \leftarrow g(\mathbf{h}_i, \theta), \forall i \in V$  ▷ GNN predictions
4  $\mathbf{r}_L \leftarrow \mathbf{y}_L - \hat{\mathbf{y}}_L$  ▷ training residuals
5  $\mathbf{y}_U^{\text{C-GNN}} \leftarrow \hat{\mathbf{y}}_U - \Gamma_{UU}^{-1} \Gamma_{UL} \mathbf{r}_L$  ▷ C-GNN predictions

```

Algorithm 2: C-GNN training (mini-batched).

Input : normalized adjacency matrix S ; features $\{\mathbf{x}_i\}$; all
training vertices L_0 , labels \mathbf{y}_L ; number of training
steps p ; batch size b
Output: optimized α, β, θ

```

1 randomly initialize  $\alpha, \beta, \theta$ 
2 for  $i \leftarrow 1$  to  $p$  do
3    $\Gamma \leftarrow \beta(\mathbf{I} - \alpha S)$ 
4    $L \leftarrow \text{subsample}(L_0, b)$  ▷ get mini-batch
5    $\mathbf{h}_i \leftarrow f(\mathbf{x}_i, \{\mathbf{x}_j : j \in N_K(i)\}, \theta), \forall i \in L$ 
6    $\hat{\mathbf{y}}_i \leftarrow g(\mathbf{h}_i, \theta), \forall i \in L$  ▷ GNN predictions
7    $\mathbf{r}_L \leftarrow \mathbf{y}_L - \hat{\mathbf{y}}_L$  ▷ training residuals
8    $\Omega \leftarrow \mathbf{r}_L^T \Gamma_{LL}^* \mathbf{r}_L - \log \det(\Gamma) + \log \det(\Gamma_{UU})$ 
9   compute  $\partial\Omega/\partial\alpha, \partial\Omega/\partial\beta, \partial\Omega/\partial\theta$  ▷ Eq. (12)
10   $\alpha, \beta, \theta \leftarrow \text{update}(\Omega, \partial\Omega/\partial\alpha, \partial\Omega/\partial\beta, \partial\Omega/\partial\theta)$ 
11 end

```

sure the limit is never realized in practice; however, we use this as motivation for a simplified version of the model in Section 2.3.

Inferring unknown labels. Now, we show how to infer unlabeled vertices assuming α, β, θ , and \mathbf{y}_L are known. If we partition Eq. (4) into the labeled and unlabeled blocks,

$$\begin{bmatrix} \mathbf{y}_L \\ \mathbf{y}_U \end{bmatrix} \sim \mathcal{N} \left(\begin{bmatrix} \hat{\mathbf{y}}_L \\ \hat{\mathbf{y}}_U \end{bmatrix}, \begin{bmatrix} \Gamma_{LL} & \Gamma_{LU} \\ \Gamma_{UL} & \Gamma_{UU} \end{bmatrix}^{-1} \right), \quad (7)$$

then conditioned on the labeled vertices L , the distribution of vertex labels on U is also a multivariate Gaussian,

$$\mathbf{y}_U \mid \mathbf{y}_L \sim \mathcal{N} \left(\hat{\mathbf{y}}_U - \Gamma_{UU}^{-1} \Gamma_{UL} \mathbf{r}_L, \Gamma_{UU}^{-1} \right). \quad (8)$$

Our model uses the expectation of this conditional distribution as the final prediction, which is given by the Gaussian mean,

$$\mathbf{y}_U^{\text{C-GNN}} = \hat{\mathbf{y}}_U - \Gamma_{UU}^{-1} \Gamma_{UL} \mathbf{r}_L. \quad (9)$$

Our inference algorithm is summarized in Algorithm 1. Next, we consider learning optimal parameters from labeled data.

Learning model parameters. Given the observed outcomes \mathbf{y}_L on L , the precision matrix parameters α, β , and GNN weights θ are learned by maximizing the marginally likelihood. In fact, the marginal distribution of the GNN residual on L is also a multivariate Gaussian [25]:

$$\mathbf{r}_L = \mathbf{y}_L - \hat{\mathbf{y}}_L \sim \mathcal{N} \left(0, \bar{\Gamma}_{LL}^{-1} \right), \quad (10)$$

where $\bar{\Gamma}_{LL} = \Gamma_{LL} - \Gamma_{LU} \Gamma_{UU}^{-1} \Gamma_{UL}$ is the corresponding precision matrix. We define the loss function as the negative log marginal

Algorithm 3: LP-GNN regression.

Input : normalized adjacency matrix S ; features $\{\mathbf{x}_i\}$;
training labels \mathbf{y}_L
Output: predicted labels $\mathbf{y}_U^{\text{LP-GNN}}$ for unknown vertices

```

1 train standard GNN, get optimized parameter  $\theta$ 
2  $\mathbf{h}_i \leftarrow f(\mathbf{x}_i, \{\mathbf{x}_j : j \in N_K(i)\}, \theta), \forall i \in V$ 
3  $\hat{\mathbf{y}}_i \leftarrow g(\mathbf{h}_i, \theta), \forall i \in V$  ▷ GNN predictions
4  $\mathbf{r}_L \leftarrow \mathbf{y}_L - \hat{\mathbf{y}}_L$  ▷ training residuals
5  $\mathbf{r}_U^{\text{est}} \leftarrow \text{LabelPropagation}(S, \mathbf{r}_L)$  ▷ e.g., Algorithm 4
6  $\mathbf{y}_U^{\text{LP-GNN}} \leftarrow \hat{\mathbf{y}}_U + \Gamma_U^{\text{est}}$ 

```

likelihood of observed labels:

$$\begin{aligned} \Omega &= -\log p(\mathbf{y}_L \mid \alpha, \beta, \theta) \\ &= \left[\mathbf{r}_L^T \bar{\Gamma}_{LL} \mathbf{r}_L - \log \det(\bar{\Gamma}_{LL}) + n \log(2\pi) \right] / 2 \\ &\propto \mathbf{r}_L^T \bar{\Gamma}_{LL} \mathbf{r}_L - \log \det(\bar{\Gamma}_{LL}) \\ &= \mathbf{r}_L^T \bar{\Gamma}_{LL} \mathbf{r}_L - \log \det(\Gamma) + \log \det(\Gamma_{UU}) \end{aligned} \quad (11)$$

Then, the loss function derivatives with respect to the model parameters take the following expression,

$$\begin{aligned} \frac{\partial \Omega}{\partial \alpha} &= \mathbf{r}_L^T \frac{\partial \bar{\Gamma}_{LL}}{\partial \alpha} \mathbf{r}_L - \text{tr} \left(\Gamma^{-1} \frac{\partial \Gamma}{\partial \alpha} \right) + \text{tr} \left(\Gamma_{UU}^{-1} \frac{\partial \Gamma_{UU}}{\partial \alpha} \right) \\ \frac{\partial \Omega}{\partial \beta} &= \mathbf{r}_L^T \frac{\partial \bar{\Gamma}_{LL}}{\partial \beta} \mathbf{r}_L - \text{tr} \left(\Gamma^{-1} \frac{\partial \Gamma}{\partial \beta} \right) + \text{tr} \left(\Gamma_{UU}^{-1} \frac{\partial \Gamma_{UU}}{\partial \beta} \right) \\ \frac{\partial \Omega}{\partial \theta} &= -2 \mathbf{r}_L^T \bar{\Gamma}_{LL} \frac{\partial \hat{\mathbf{y}}_L}{\partial \theta}, \end{aligned} \quad (12)$$

where $\partial \hat{\mathbf{y}}_L / \partial \theta$ can be computed with back-propagation, and

$$\begin{aligned} \frac{\partial \bar{\Gamma}_{LL}}{\partial \alpha} &= \frac{\partial \Gamma_{LL}}{\partial \alpha} - \frac{\partial \Gamma_{LU}}{\partial \alpha} \Gamma_{UU}^{-1} \Gamma_{UL} + \Gamma_{LU} \Gamma_{UU}^{-1} \frac{\partial \Gamma_{UU}}{\partial \alpha} \Gamma_{UU}^{-1} \Gamma_{UL} \\ &\quad - \Gamma_{LU} \Gamma_{UU}^{-1} \frac{\partial \Gamma_{UL}}{\partial \alpha} \\ \frac{\partial \bar{\Gamma}_{LL}}{\partial \beta} &= \frac{\partial \Gamma_{LL}}{\partial \beta} - \frac{\partial \Gamma_{LU}}{\partial \beta} \Gamma_{UU}^{-1} \Gamma_{UL} + \Gamma_{LU} \Gamma_{UU}^{-1} \frac{\partial \Gamma_{UU}}{\partial \beta} \Gamma_{UU}^{-1} \Gamma_{UL} \\ &\quad - \Gamma_{LU} \Gamma_{UU}^{-1} \frac{\partial \Gamma_{UL}}{\partial \beta}. \end{aligned} \quad (13)$$

Finally, let P, Q denote two arbitrary sets of vertices, the derivatives of each precision matrix block Γ_{PQ} are given by $\partial \Gamma_{PQ} / \partial \alpha = -\beta S_{PQ}$ and $\partial \Gamma_{PQ} / \partial \beta = \Gamma_{PQ} / \beta$. In practice, we employ a mini-batch sampling for better memory efficiency, and we maximize the marginal likelihood of a mini-batch at each training step (Algorithm 2).

One remaining issues is the computation cost. Standard matrix factorization-based algorithms for computing the matrix inverse and log determinant have complexity cubic in the number of vertices, which is computationally prohibitive for graphs beyond a few thousand vertices. In Section 3, we show how to reduce these computations to linear in the number of edges, using recent tricks in stochastic trace estimation. Next, we offer an even cheaper alternative that works well when α is close to 1.

2.3 A Simple Propagation-based Algorithm

Our framework is inspired in part by label propagation [38, 40], where the neighboring correlation is always assumed to be positive. In fact, if we fix $\alpha = 1$ and replace the base GNN regressor with one

that gives uniform 0 prediction for all vertices, our method reduces to a variant of label propagation that uses the normalized Laplacian matrix (see details in Appendix A.1), which is somewhat expected given known connections between Gaussian Process regression (kriging) and graph-based semi-supervised learning [35].

This observation motivates an extremely simple version of our method, which we call LP-GNN (Algorithm 3): (i) train a standard GNN; (ii) run label propagation from the residuals on labeled vertices; (iii) add the propagated result to the GNN predictions. LP-GNN is a light-weight framework for data where residual correlation is strong and positive, and in principle, any label propagation method could be employed. We show in Section 4 that this provides substantial improvements over a GNN in many cases but is less successful than C-GNN.

2.4 Extension to Multiple Edge Types

Our model can also be extended to study graphs with multiple edge types. For instance, later in Section 4.2, we consider a traffic graph where different pairs of lanes, based on their orientations, are connected with different types of edges. In this case, we decompose the total adjacency matrix as $\mathbf{A} = \sum_i \mathbf{A}^{(i)}$, where $\mathbf{A}^{(i)}$ includes all the edges of type- i . Then, denoting $\mathbf{S}^{(i)} = \mathbf{D}^{-1/2} \mathbf{A}^{(i)} \mathbf{D}^{-1/2}$, we parametrize the precision matrix as

$$\Gamma = \beta(\mathbf{I} - \sum_i \alpha_i \mathbf{S}^{(i)}). \quad (14)$$

Following the same logic as in Section 2.2, the precision matrix above is still positive definite if $-1 < \alpha_i < 1$ for all i , and the loss function derivatives with respect to $\{\alpha_i\}$ take similar expressions to the original model. The extended model provides finer grained descriptions for interactions among neighboring vertices. Our experiments show the extended model captures the difference in correlation strengths for different types of edges in the traffic network, as well as improving the regression accuracy.

3 FAST MODEL OPTIMIZATION

We have introduced a simple and interpretable framework to exploit residual correlations. The model parameters are learned by minimizing the negative log marginal likelihood loss with a gradient-based method; however, the cubic scaling computational cost of standard algorithms for evaluating the log determinant limits the model’s applicability to large-scale networks. To this end, we show how to use stochastic estimation for the log determinant and its derivatives, which takes full advantage of our sparse precision matrix parametrization and reduces computational cost to $\mathcal{O}(m)$.

3.1 Efficient Log-determinant Estimation

The major computational cost in our framework boils down to three types of matrix operations: (i) solving the linear system $\Gamma^{-1} \mathbf{z}$; (ii) computing matrix trace $\text{tr}(\Gamma^{-1} \frac{\partial \Gamma}{\partial \alpha})$; and (iii) computing log determinate $\log \det(\Gamma)$.⁵ Next, we show how our precision matrix parametrization allows those operations to be computed efficiently using conjugate gradients (CG), stochastic trace estimation, and Lanczos quadrature [2, 7, 10, 29].

⁵We focus on evaluating $\log \det(\Gamma)$ and $\frac{\partial \log \det(\Gamma)}{\partial \alpha}$ in our analysis, but the results easily generalize to $\log \det(\Gamma_{UU})$ and $\frac{\partial \log \det(\Gamma_{UU})}{\partial \beta}$.

Conjugate Gradients (CG) solution of $\Gamma^{-1} \mathbf{z}$. CG is an iterative algorithm for solving linear systems, where the matrix is symmetric and positive definite. Each CG iteration computes one matrix vector multiplication and a handful of vector operations, therefore solving $\Gamma^{-1} \mathbf{z}$ by running k iterations of CG requires $\mathcal{O}(km)$ operations, where m is the number of edges in the graph. The convergence rate of CG depends on the condition number of Γ , which is defined as the ratio between the largest and smallest eigenvalues $\kappa(\Gamma) = \lambda_{\max}(\Gamma)/\lambda_{\min}(\Gamma)$. In particular, for a fixed error tolerance, CG is guaranteed to converge in $\mathcal{O}(\sqrt{\kappa(\Gamma)})$ iterations. Next, we provide an upper bound on $\kappa(\Gamma)$, which justifies using a fixed number of k iterations in our CG implementation.

Since the eigenvalues of the normalized adjacency matrix \mathbf{S} are bounded between -1.0 and 1.0 [5], we can bound the extreme eigenvalues of the precision matrix as follows:

$$\begin{aligned} \lambda_{\max}(\Gamma) &= \beta \lambda_{\max}(\mathbf{I} - \alpha \mathbf{S}) < \beta [\lambda_{\max}(\mathbf{I}) + \lambda_{\max}(-\alpha \mathbf{S})] = \beta(1 + |\alpha|) \\ \lambda_{\min}(\Gamma) &= \beta \lambda_{\min} \left[(1 - |\alpha|) \mathbf{I} + |\alpha| \left(\mathbf{I} - \frac{\alpha}{|\alpha|} \mathbf{S} \right) \right] > \beta(1 - |\alpha|) \end{aligned} \quad (15)$$

Then, the upper bound of the condition number is given by

$$\kappa(\Gamma) = \lambda_{\max}(\Gamma)/\lambda_{\min}(\Gamma) < (1 + |\alpha|)/(1 - |\alpha|), \quad (16)$$

which does not depend on the graph topology. (This upper bound also applies to Γ_{UU} via the eigenvalue interlacing theorem.) Therefore, by further constraining $|\alpha| < 1 - \eta$ for a small positive constant η , CG algorithm converges in $\mathcal{O}(\sqrt{2/\eta})$ iterations. We will verify numerically in Section 3.2 that CG indeed converges in a couple dozen iterations for our framework.

Stochastic Estimation of $\text{tr}(\Gamma^{-1} \frac{\partial \Gamma}{\partial \alpha})$. The stochastic trace estimator is an established method for approximating the trace of a matrix function [2, 17]. Given a Gaussian random vector $\mathbf{z} \sim \mathcal{N}(0, \mathbf{I})$ with $E[z_i z_j] = \delta_{ij}$, where δ_{ij} is the Kronecker delta function,

$$\mathbb{E}[\mathbf{z}^T \mathbf{M} \mathbf{z}] = \mathbb{E}[\sum_i z_i^2 M_{ii} + \sum_{i \neq j} z_i z_j M_{ij}] = \sum_i M_{ii} \quad (17)$$

gives the unbiased trace estimation for any matrix \mathbf{M} . This allows us to estimate $\text{tr}(\Gamma^{-1} \frac{\partial \Gamma}{\partial \alpha})$ without explicitly forming Γ^{-1} . In practice, given a series of T independent and identically sampled Gaussian random vectors $\mathbf{z}_t \sim \mathcal{N}(0, \mathbf{I})$, we estimate the matrix trace by

$$\text{tr}(\Gamma^{-1} \frac{\partial \Gamma}{\partial \alpha}) = \mathbb{E} \left[\mathbf{z}_t^T \Gamma^{-1} \frac{\partial \Gamma}{\partial \alpha} \mathbf{z}_t \right] \approx \frac{1}{T} \sum_{t=1}^T (\Gamma^{-1} \mathbf{z}_t)^T \left(\frac{\partial \Gamma}{\partial \alpha} \mathbf{z}_t \right), \quad (18)$$

which would require calling the conjugate gradient solver T times with the same matrix Γ but different right-hand-sides.

Stochastic Lanczos quadrature for $\log \det(\Gamma)$. We adopt the approach of Ubaru et al. for approximating the log-determinant, which estimates the trace of the logarithm of the matrix [29]:

$$\begin{aligned} \log \det(\Gamma) &= \text{tr}(\log \Gamma) \approx \frac{1}{T} \sum_{t=1}^T \mathbf{z}_t^T \log \Gamma \mathbf{z}_t \\ &= \frac{1}{T} \sum_{t=1}^T \mathbf{z}_t^T \mathbf{Q} \log \Lambda \mathbf{Q}^T \mathbf{z}_t \\ &= \frac{1}{T} \sum_{t=1}^T \sum_{i=1}^n \mu_{ti}^2 \cdot \log \lambda_i(\Gamma), \end{aligned} \quad (19)$$

where $\Gamma = \mathbf{Q} \Lambda \mathbf{Q}^T$ is the eigen-decomposition, and μ_{ti} is the projected length of \mathbf{z}_t on the i -th eigenvector of Γ . The expression $\sum_i \mu_{ti}^2 \cdot \log \lambda_i(\Gamma)$ can be considered as a Riemann-Stieltjes integral, and is further approximated with Gaussian quadrature:

$$\sum_{i=1}^n \mu_{ti}^2 \cdot \log \lambda_i(\Gamma) \approx \sum_{i=1}^k w_{ti}^2 \cdot \log \xi_{ti}, \quad (20)$$

where the optimal nodes $\{\xi_{ti}\}$ and weights $\{w_{ti}\}$ for numerical integration are determined as follows. First, run k steps of the Lanczos algorithm with Γ and initial vector \mathbf{z}_t to get $\mathbf{V}_t^T \Gamma \mathbf{V}_t = \mathbf{T}_t$. Then, perform the eigen-decomposition of the tri-diagonal matrix $\mathbf{T}_t = \mathbf{P}_t \Xi_t \mathbf{P}_t^T$. Each integration node is an eigenvalue of \mathbf{T}_t whose weight is the first element of each corresponding eigenvector:

$$\xi_{ti} = (\Xi_t)_{ii}, \quad w_{ti} = \sqrt{n} \cdot (\mathbf{P}_t)_{1i} \quad (21)$$

We point the readers to Ubaru et al. for a complete derivation [29].

Implementation and algorithm complexity. Both the CG and Lanczos algorithms are Krylov subspace methods, and their convergence essentially depends on the condition number [32]. Since the condition number in our precision matrix parametrization is bounded, we use a fixed number of k iterations in both algorithms. Furthermore, the error of the stochastic trace estimator decrease with the number of trial vectors T as $O(T^{-1/2})$, regardless of the graph topology, and we also use a fixed number of T vectors.

We summarize the overall complexity of the proposed method for evaluating Eqs. (11) and (12) in each optimization step. Computing \hat{y}_L and $\partial \hat{y}_L / \partial \theta$ through forward and back propagation takes $O(n)$ operations (assuming constant-size neighborhood subsampling in GNN implementations). Evaluating the quadratic forms in Eq. (12) invokes a constant number of calls (8 in our case) to the CG solver, which takes $O(mk)$ operations. The trace estimations $\text{tr}(\Gamma^{-1} \frac{\partial \Gamma}{\partial \alpha})$ invokes T calls to the CG solver, which takes $O(mkT)$ operations. The log-determinant estimation $\log \det(\Gamma)$ invokes T calls to the Lanczos algorithm, which takes $O(mkT)$ operations. Finally, the eigen-decomposition of the k -by- k tri-diagonal matrices $\{\mathbf{T}_t\}_{t=1}^T$ takes $O(Tk^2)$ operations. We choose $T = 128, k = 32$ as the default hyperparameters, independent of the size of the graph for an overall complexity of $O(m)$, i.e., linear in the number of edges.

Stochastic estimation of the log determinant and its derivatives of the covariance matrix has been considered in the context of Gaussian Processes [13], where a similar computational scheme is used to reduce the complexity from $O(n^3)$ to $O(n^2)$. Our model further benefits from the sparse and well-conditioned precision matrix parametrization, which results in linear time algorithm for the objective function and its gradients. We implement the log-determinant estimation function in Julia using the Flux.jl automatic differentiation package [19], which automatically tracks the function value and derivatives with computational graph (Appendix A.2). We also adapt techniques proposed by Gardner et al. for reusing computation and improving cache efficiency [13].

3.2 Approximation Validation

In the previous section, we proposed to use stochastic trace estimation for computing log determinant. We now evaluate the performance dependence of those estimations on the hyperparameters T and k . We find that the proposed scheme gives accurate and unbiased estimation for log determinant and its derivatives for modest values of T and k , and we empirically show linear scaling.

Accuracy in estimating log determinant and its derivatives. To test our fast algorithms, we sample a Watts-Strogatz graph [33] with 500 vertices and average vertex degree 10. We randomly select 50% vertices as labeled, and compute the marginal precision matrix $\tilde{\Gamma}_{LL}$ with $\alpha = 0.999$ and $\beta = 1.0$, which corresponds to

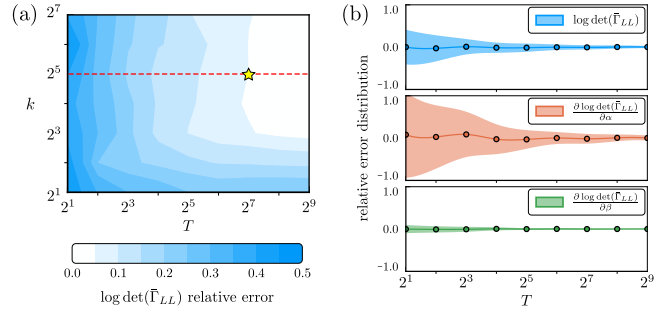


Figure 3: Estimation error as a function of accuracy hyperparameters. (a) Relative error of log determinant estimation. The yellow star represents default hyperparameters. (b) Relative error distribution along the red dashed line in (a) of the log determinant and its derivatives as a function of T .

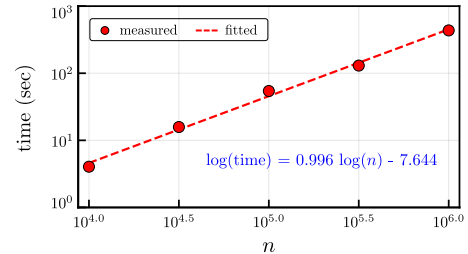


Figure 4: Linear scaling of the stochastic estimation algorithm using random Watts-Strogatz graphs, where the average degree in each graph is 10. Measured times are circles, and the dashed line is the linear fit (coefficients in blue).

a very ill-conditioned parametrization. To understand how the quality of the approximation depends on the accuracy hyperparameters, we compare our stochastic algorithm output to “ground truth” log-determinant and derivatives obtained from factorization-based algorithms. The estimation accuracy is measured by the root mean square relative error over 100 runs (for various T, k ; Fig. 3). Under the default hyperparameters ($T = 128, k = 32$), the relative error between log-determinant estimation and the ground truth is less than 5%. Moreover, our algorithm produces unbiased estimates for the derivatives with respect to α and β , which enables us to confidently use stochastic gradient methods for learning those parameters.

Scalability of stochastic estimation. Now, we validate the computational complexity of the proposed algorithm. We run our algorithm on a series of Watts-Strogatz graphs with increasing number of vertices, where the average degree in each graph is fixed to be 10. Fig. 4 shows that the empirical running time grows linearly with the size of the graph, as indicated by the slope of the fitted curve.

4 NUMERICAL EXPERIMENTS

Now that we have developed efficient algorithms for optimizing model parameters, we use our model for label prediction tasks in synthetic and real-world attributed graphs. Our model learns both positive and negative residual correlations from real-world data, which substantially boosts the regression accuracy and also provides insights about the correlation among neighboring vertices.

4.1 Data

Our model and the baselines are tested on the following graphs (see Appendix A.4 for additional datasets details).

Ising model. The Ising model is a widely-used random model in statistical physics [6], and we consider vertices on a 35×35 grid graph. The spin of each vertex is either up (+1.0) or down (-1.0), which tends to align with an external field but is also influenced by neighboring spins. The neighboring spins are likely to be parallel if their interaction is set to be positive, and anti-parallel otherwise. We use Ising model samples from these two settings and denote them by Ising(+) and Ising(-), respectively, providing synthetic datasets with clear positive and negative correlations in labels. We use the grid coordinates as vertex features to predict vertex spins.

U.S. Election Maps. The election map data is in Fig. 2, where vertices are counties in the U.S. and edges connect bordering counties. Each county has demographic and election statistics.⁶ We use these as both features and outcomes: in each experiment, we select one statistic as the outcome; the remaining are vertex features. We use 2012 and 2016 statistics. The former is used for the transductive experiments, and both are used for the inductive experiments.

Transportation networks. The transportation networks contain traffic data in the cities of Anaheim and Chicago⁷. Each vertex represents a directed lane, and two lanes that meet at same intersections are connected. Since the lanes are directed, we create two type of edges: lanes that meet head-to-tail are connected by type-1 edge, and lanes that meet head-to-head or tail-to-tail are connected by type-2 edge. For this, we use our extended model from Section 2.4. The length, capacity, and speed limit of each lanes are used as features to predict traffic flows on the lanes.

Sexual interactions. This dataset is a sexual interaction network amongst 1888 individuals from a study on HIV transmission [22]. We use race and sexual orientation as vertex features to predict the gender of each person (+1.0 for male and -1.0 for female). Most sexual interactions are heterosexual, producing negative correlations in the label distribution.

Twitch social network. The Twitch dataset represents online friendships amongst Twitch streamers in Portugal [26]. Vertex features are principal components from statistics such as the games played and liked, location, and streaming habits. The goal is to predict the logarithm of the number of viewers for each streamer.

4.2 Transductive Learning

We first consider the transductive setting, where the training and testing vertices are from the same graph. We find that our C-GNN framework greatly improves prediction accuracy over GNNs.

Methods and baselines. We use a 2-layer GraphSAGE GNN with ReLU activations and mean-aggregation [14] as the base predictor in our framework. (Other GNN architecture provide similar results; see Appendix A.5.) We compare C-GNN against label propagation (LP) [40], a multi-layer perceptron (MLP; architecture details in Appendix A.3), the base GNN, and the LP-GNN algorithm from Section 2.3. LP assumes and takes advantage of positive label correlation among neighboring vertices, but it does not use vertex

⁶Data from www.ers.usda.gov/data-products/county-level-data-sets/.

⁷Data from <https://github.com/bstabler/TransportationNetworks>.

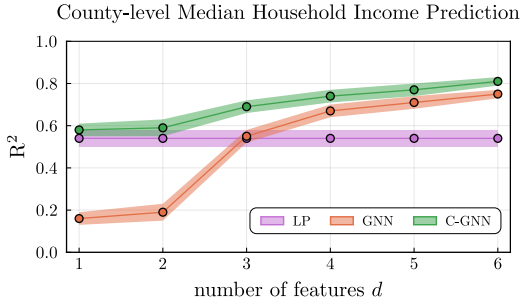


Figure 5: Transductive learning accuracy for county-level median household incomes, as a function of the number of included features. Label propagation (LP) can work well with few features, while the GNN can work well with many features; however, C-GNN outperforms both in all cases.

features. On the other hand, the MLP ignores the label correlations, and only uses the features of a given vertex to predict its label. We also tested how effective is our correlation framework for improving the performance of MLP by replacing the GNN base regressor in C-GNN and LP-GNN methods with the MLP base regressor. The resulting methods are denoted as C-MLP and LP-MLP.

Setup and performance metric. For each graph, we normalize each vertex feature to have zero mean and unit standard deviation, and randomly split the vertices into 60% for training, 20% for validation, and 20% for testing. The GNN parameters are trained using the ADAM optimizer with default learning rate, while the model parameters α, β are optimized with gradient descent along with the GNN parameters. For the Ising model and sexual interaction datasets, the vertex labels are binary, therefore we threshold the regression output at 0 and use binary classification accuracy as the performance metric. For the rest of datasets, we use coefficients of determination R^2 to measure accuracy. Each combination of method and dataset is repeated 10 times with different random seeds, and the mean and standard deviation of the accuracies are recorded.

Main results. Table 1 summarizes the results. C-GNN substantially improves the prediction accuracy over GNN for all datasets: the C-GNN mean classification accuracy is 0.82 over the Ising spin and sexual interaction datasets, and the mean R^2 is 0.75 over the remaining datasets, while the GNN mean classification and R^2 accuracies were 0.67 and 0.66, respectively. Moreover, our LP-GNN also performs very well on most of the datasets, with performance on par with C-GNN in five datasets and out-performing the standard GNN in 8 out of 10 datasets. The two datasets on which it performs poorly are Ising(-) and the sexually interaction network, where the labels of connected vertices are likely to be negatively correlated; this is expected since the LP-GNN model assumes positive correlations amongst neighboring vertices.

Interestingly, the performance of the MLP can be improved substantially with our framework. In fact, C-MLP is often much better than a standard GNN. This is evidence that oftentimes more performance can be gained from exploring label correlation as opposed to sophisticated feature aggregation.

The learned parameters also reveal interaction types. The learned $\{\alpha_i\}$ are all positive except for the Ising(-) and sexual datasets, where the vertex labels are negatively correlated. Moreover, for the traffic

Table 1: Transductive learning accuracy of our C-GNN and LP-GNN models compared to competing baselines. The best accuracy is in green. Our C-GNN outperforms GNN on all datasets, often by a substantial margin. Even C-MLP, which does not use neighbor features, outperforms GNN in many cases, highlighting the importance of label correlation. LP, C0-MLP and C0-GNN assume positive label correlation among neighboring vertices and perform poorly for datasets where most edges encode negative interactions, as highlighted in orange. We also report the learned $\{\alpha_i\}$ values from C-GNN.

Dataset	n	m	LP	MLP	LP-MLP	C-MLP	GNN	LP-GNN	C-GNN	$\{\alpha_i\}$
Ising(+)	1.2K	2.4K	0.76 \pm 0.02	0.68 \pm 0.03	0.76 \pm 0.02	0.76 \pm 0.02	0.67 \pm 0.04	0.76 \pm 0.02	0.76 \pm 0.02	+0.89
Ising(-)	1.2K	2.4K	0.30 \pm 0.03	0.47 \pm 0.02	0.30 \pm 0.03	0.77 \pm 0.03	0.47 \pm 0.03	0.30 \pm 0.03	0.77 \pm 0.03	-0.93
income	3.2K	12.7K	0.54 \pm 0.04	0.64 \pm 0.03	0.73 \pm 0.03	0.74 \pm 0.03	0.75 \pm 0.03	0.81 \pm 0.03	0.81 \pm 0.02	+0.92
education	3.2K	12.7K	0.36 \pm 0.05	0.67 \pm 0.03	0.71 \pm 0.02	0.72 \pm 0.02	0.70 \pm 0.02	0.72 \pm 0.03	0.72 \pm 0.03	+0.78
unemployment	3.2K	12.7K	0.70 \pm 0.03	0.43 \pm 0.05	0.69 \pm 0.04	0.77 \pm 0.03	0.55 \pm 0.04	0.75 \pm 0.05	0.78 \pm 0.03	+0.99
election	3.2K	12.7K	0.58 \pm 0.02	0.37 \pm 0.02	0.61 \pm 0.03	0.63 \pm 0.03	0.51 \pm 0.04	0.69 \pm 0.03	0.69 \pm 0.03	+0.95
Anaheim	914	3.8K	0.49 \pm 0.08	0.75 \pm 0.02	0.81 \pm 0.04	0.82 \pm 0.03	0.76 \pm 0.03	0.81 \pm 0.04	0.82 \pm 0.03	+0.95, +0.17
Chicago	2.2K	15.1K	0.59 \pm 0.05	0.60 \pm 0.05	0.65 \pm 0.06	0.65 \pm 0.05	0.68 \pm 0.04	0.72 \pm 0.04	0.71 \pm 0.04	+0.85, +0.68
sexual	1.9K	2.1K	0.37 \pm 0.06	0.68 \pm 0.02	0.64 \pm 0.03	0.83 \pm 0.03	0.88 \pm 0.02	0.86 \pm 0.02	0.93 \pm 0.01	-0.98
Twitch-PT	1.9K	31.3K	0.00 \pm 0.04	0.61 \pm 0.03	0.60 \pm 0.04	0.66 \pm 0.03	0.69 \pm 0.03	0.69 \pm 0.03	0.74 \pm 0.03	+0.99

graph, the learned $\alpha_1 > \alpha_2$ indicates traffics on two lanes with head-to-tail connection are more strongly correlated, since a vehicle can directly move from one lane to another.

Understanding performance better. We perform a more in-depth analysis for predicting county-level median household income. This dataset has six features (migration rate, birth rate, death rate, education level, unemployment rate, and election outcome) in total, and we use the first d for income prediction, comparing against LP and GNN (Fig. 5). The GNN performs poorly for small d , but gradually surpasses LP as more features are available. Our C-GNN method outperforms both regardless of d , although the performance gap between C-GNN and GNN narrows as d increases. These results highlight that, if features are only mildly predictive, accounting for label correlation can have an enormous benefit.

4.3 Inductive Learning

We now consider the inductive setting, where a model is trained on vertex labels from one graph G and tested on an unseen graph G' . This setting is useful when both graphs have similar properties, but vertex labels in G' are more expensive to obtain. In particular, we consider the scenario where a small fraction of vertex labels in G' are available and demonstrate how our framework allows using those extra labels to improve regression accuracy. We denote the labeled and unlabeled vertices in G' as L' and U' .

Datasets and methods. We use the Ising model and election map datasets for inductive learning experiments. In the former, the spin configurations on G and G' are simulated under the same Ising model setting. In the latter, we train with the 2012 data and test on the 2016 election map. Our proposed framework C-GNN is compared against GNN and MLP. In particular, C-GNN is trained using 60% vertex labels from G , and tested directly on U' by conditioning on the vertex labels of L' . The GNN and MLP are first trained on G ; to provide a more fair comparison, we then use the learned parameters as the initial guess for G' , and optimize the model further with the labels on L' .

Results. We test the performance of our framework and the baselines for different sizes of L' (Fig. 6). C-GNN and GNN gives the

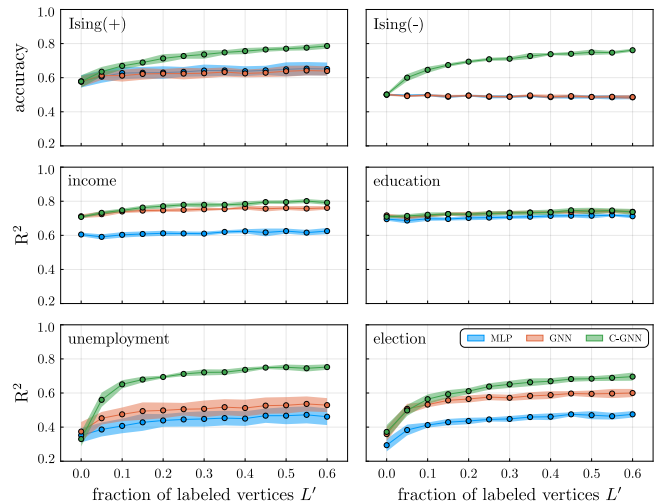


Figure 6: Inductive learning accuracy with a fraction of labeled vertices in the new graph. C-GNN is able to utilize the extra labels more effectively than the baselines, and it does not need neural network fine-tuning.

same prediction accuracy if no vertex label on G' is available, but, as the number of labeled points increases, C-GNN outperforms the baselines by large margins on multiple datasets. This indicates that the learned residual correlation generalizes well to unseen graphs. Household income and education prediction do not benefit much from our framework, partially because those statistics are relatively stable over time, and the models trained on 2012 data are already a good proxy for 2016. Remarkably, C-GNN works well without fine-tuning the neural network parameters on the new labels of L' , indicating that the feature-label mapping oftentimes shifts from G to G' collectively amongst neighboring vertices.

5 RELATED WORK

By now, semi-supervised learning on graphs has been extensively studied [18, 20, 38, 40]. Label propagation or diffusion “distributes” observed vertex labels throughout the graph [38, 40], but were not

designed to incorporate additional vertex features. Laplacian Regularization [1] and Manifold regularization [3] propose to augment feature-based supervised learning methods with an unsupervised loss function that minimize differences between connected vertices. These methods assume neighboring vertices should have similar labels, which is true in many applications.

There are direct models of correlation structure for graph-based semi-supervised learning [35]; such approaches are more computationally expensive and not amenable to joint learning with GNN parameters. The marginalized Gaussian conditional random field (m-GCRF) [28] is closer to our approach, using a CRF to model the label distribution given the vertex features, which reduces to Gaussian distribution with sparse precision matrices under the right choice of potential function. In contrast, we model the correlation of regression residuals instead of the outcomes themselves, and our precision matrix parameterization enables linear-time learning.

The inability of existing GNN approaches to capture label correlations has been discussed in the classification setting. Recent proposals include graph Markov neural networks [24] and conditional graph neural fields [12], which use a CRF to model the joint distribution of vertex classes; as well as positional GNNs [37], which use a heuristic of letting GNN aggregation parameters depend on distances to anchor nodes. With the CRF approaches, the joint likelihood does not have a close form expression, and such models are trained by maximizing the pseudo-likelihood with the expectation-maximization algorithm. The regression setting here is more mathematically convenient: an unbiased exact joint likelihood estimate can be quickly computed, and the outcome has an interpretable decomposition into base prediction and residual.

6 DISCUSSION

Our semi-supervised regression framework combines the advantages of GNNs and label propagation to get the most out of both vertex feature information and outcome correlations. Our experiments show that accounting for outcome correlations can give enormous performance gains, especially in cases where the base prediction by a GNN is only mildly accurate. This says that label correlation structure can provide information complementary (rather than redundant) to vertex features in some datasets. Understanding this more formally is an interesting avenue for future research.

Our C-GNN uses only a few parameters to model the label correlation structure, and learns the direction and strength of correlations with highly efficient algorithms. The model also enables us to measure uncertainty in predictions, although we did not focus on this. The C-GNN can model more types of data and requires some careful numerical algorithms to scale well; our simplified LP-GNN approach offers a light-weight add-on to any GNN implementation that can substantially boost performance in many cases.

ACKNOWLEDGMENTS

This research was supported by NSF Award DMS-1830274, ARO Award W911NF19-1-0057, and ARO MURI.

REFERENCES

[1] Rie Kubota Ando and Tong Zhang. 2006. Learning on Graph with Laplacian Regularization. In *NeurIPS*.

[2] Haim Avron and Sivan Toledo. 2011. Randomized Algorithms for Estimating the Trace of an Implicit Symmetric Positive Semi-Definite Matrix. *J. ACM* (2011).

[3] Mikhail Belkin, Partha Niyogi, and Vikas Sindhwani. 2006. Manifold Regularization: A Geometric Framework for Learning from Labeled and Unlabeled Examples. *J. Mach. Learn. Res.* (2006).

[4] Jie Chen, Tengfei Ma, and Cao Xiao. 2018. FastGCN: Fast Learning with Graph Convolutional Networks via Importance Sampling. In *ICLR*.

[5] Fan RK Chung and Fan Chung Graham. 1997. *Spectral graph theory*. Number 92. American Mathematical Soc.

[6] Barry A. Cipra. 1987. An Introduction to the Ising Model. *Am. Math. Monthly* (1987).

[7] Kun Dong, Austin R Benson, and David Bindel. 2019. Network density of states. In *KDD*. 1152–1161.

[8] David Easley and Jon Kleinberg. 2010. *Networks, Crowds, and Markets: Reasoning About a Highly Connected World*. Cambridge University Press.

[9] Juan Fernández-Gracia, Krzysztof Suchecki, José J. Ramasco, Maxi San Miguel, and Víctor M. Eguíluz. 2014. Is the Voter Model a Model for Voters? *Physical Review Letters* (2014).

[10] JK Fitzsimons, MA Osborne, SJ Roberts, and JF Fitzsimons. 2018. Improved stochastic trace estimation using mutually unbiased bases. AUAJ Press.

[11] Jerome Friedman, Trevor Hastie, and Robert Tibshirani. 2001. *The elements of statistical learning*. Vol. 1. Springer series in statistics New York.

[12] Hongchang Gao, Jian Pei, and Heng Huang. 2019. Conditional Random Field Enhanced Graph Convolutional Neural Networks. In *KDD*.

[13] Jacob Gardner, Geoff Pleiss, Kilian Q Weinberger, David Bindel, and Andrew G Wilson. 2018. GPYtorch: Blackbox Matrix-Matrix Gaussian Process Inference with GPU Acceleration. In *NeurIPS*.

[14] William L. Hamilton, Rex Ying, and Jure Leskovec. 2017. Inductive Representation Learning on Large Graphs. In *NeurIPS*.

[15] William L. Hamilton, Rex Ying, and Jure Leskovec. 2017. Representation learning on graphs: Methods and applications. *IEEE Data Engineering Bulletin* (2017).

[16] Ken Hayami. 2018. Convergence of the Conjugate Gradient Method on Singular Systems. *arXiv e-prints* (2018).

[17] M.F. Hutchinson. 1989. A Stochastic Estimator of the Trace of the Influence Matrix for Laplacian Smoothing Splines. *Communications in Statistics - Simulation and Computation* (1989).

[18] Rania Ibrahim and David Gleich. 2019. Nonlinear Diffusion for Community Detection and Semi-Supervised Learning. In *WWW*.

[19] Mike Innes. 2018. Flux: Elegant Machine Learning with Julia. *Journal of Open Source Software* (2018).

[20] Junteng Jia, Michael T. Schaub, Santiago Segarra, and Austin R. Benson. 2019. Graph-Based Semi-Supervised & Active Learning for Edge Flows. In *KDD*.

[21] Thomas N. Kipf and Max Welling. 2017. Semi-Supervised Classification with Graph Convolutional Networks. In *ICLR*.

[22] Martina Morris and Richard Rothenberg. 2011. *HIV Transmission Network Meta-study Project: An Archive of Data From Eight Network Studies, 1988–2001*. Inter-university Consortium for Political and Social Research.

[23] Mark Newman. 2010. *Networks: An Introduction*. Oxford University Press.

[24] Meng Qu, Yoshua Bengio, and Jian Tang. 2019. GMNN: Graph Markov Neural Networks. *ICML*.

[25] Carl Edward Rasmussen. 2003. Gaussian processes in machine learning. In *Summer School on Machine Learning*. Springer, 63–71.

[26] Benedek Rozemberczki, Carl Allen, and Rik Sarkar. 2019. Multi-scale Attributed Node Embedding. *arXiv preprint arXiv:1909.13021* (2019).

[27] Cosma Shalizi. 2015. Weighted and Generalized Least Squares.

[28] Jelena Stojanovic, Milos Jovanovic, Djordje Gligorijevic, and Zoran Obradovic. 2015. Semi-supervised learning for structured regression on partially observed attributed graphs. In *ICDM*.

[29] Shashanka Ubaru, Jie Chen, and Yousef Saad. 2017. Fast Estimation of $\text{tr}(f(A))$ via Stochastic Lanczos Quadrature. *SIAMX* (2017).

[30] Rianne van den Berg, Thomas N. Kipf, and Max Welling. 2018. Graph Convolutional Matrix Completion. *KDD Deep Learning Day* (2018).

[31] Petar Veličković, Guillem Cucurull, Arantxa Casanova, Adriana Romero, Pietro Liò, and Yoshua Bengio. 2018. Graph Attention Networks. *ICLR* (2018).

[32] David S. Watkins. 2007. *The Matrix Eigenvalue Problem*. Society for Industrial and Applied Mathematics.

[33] Duncan J Watts and Steven H Strogatz. 1998. Collective dynamics of ‘small-world’ networks. *Nature* (1998).

[34] Keyulu Xu, Weihua Hu, Jure Leskovec, and Stefanie Jegelka. 2019. How Powerful are Graph Neural Networks?. In *ICLR*.

[35] Ya Xu, Justin S Dyer, and Art B Owen. 2010. Empirical Stationary Correlations for Semi-supervised Learning on Graphs: Network Modeling. *The Annals of Applied Statistics* (2010).

[36] Rex Ying, Ruining He, Kaifeng Chen, Pong Eksombatchai, William L. Hamilton, and Jure Leskovec. 2018. Graph Convolutional Neural Networks for Web-Scale Recommender Systems. In *KDD*.

[37] Jiaxuan You, Rex Ying, and Jure Leskovec. 2019. Position-aware graph neural networks. *ICML* (2019).

- [38] Dengyong Zhou, Olivier Bousquet, Thomas N. Lal, Jason Weston, and Bernhard Schölkopf. 2004. Learning with Local and Global Consistency. In *NeurIPS*.
- [39] Jie Zhou, Ganqu Cui, Zhengyan Zhang, Cheng Yang, Zhiyuan Liu, Lifeng Wang, Changcheng Li, and Maosong Sun. 2018. Graph neural networks: A review of methods and applications. *arXiv preprint arXiv:1812.08434* (2018).
- [40] Xiaojin Zhu, Zoubin Ghahramani, and John Lafferty. 2003. Semi-Supervised Learning Using Gaussian Fields and Harmonic Functions. In *ICML*.

A APPENDIX

Here we provide some implementation details of our methods to help readers reproduce and further understand the algorithms and experiments in this paper. All of the algorithms used in this paper are implemented in Julia 1.2. The source code, data, and experiments can be found at <https://github.com/000Justin000/gnn-residual-correlation.git>.

A.1 Label Propagation Algorithm

Given targets on the training vertices \mathbf{z}_L , LP compute the targets on the testing vertices \mathbf{z}_U with the following constrained minimization:

$$\mathbf{z}^{\text{LP}} = \arg \min_{\hat{\mathbf{z}}} \hat{\mathbf{z}}^T \mathcal{L} \hat{\mathbf{z}} \quad \text{s.t.} \quad \hat{\mathbf{z}}_L = \mathbf{z}_L \quad (22)$$

where $\mathcal{L} = \mathbf{I} - \mathbf{S}$ is the normalized Laplacian matrix. This is equivalent to the method by Zhu et al. [40], just with the normalized Laplacian instead of the combinatorial Laplacian, which is nearly the same as the approach by Zhou et al. [38]. The solution on the unlabeled vertices is

$$\mathbf{z}_U^{\text{LP}} = -\mathcal{L}_{UU}^{-1} \mathcal{L}_{UL} \mathbf{z}_L, \quad (23)$$

which we can compute with CG. If L and U are disconnected, \mathcal{L}_{UU} is singular. Then starting with an all-zero initial guess, CG converges to the minimal norm solution that satisfies Eq. (22) [16]. The entire algorithm is summarized in Algorithm 4.

Algorithm 4: Label Propagation.

Input : normalized adjacency matrix \mathbf{S} ; training targets \mathbf{z}_L (label or residual);

Output: predicted targets \mathbf{z}_U^{LP} for unknown vertices

- 1 $\mathcal{L} \leftarrow \mathbf{I} - \mathbf{S}$ ▷ precision matrix
 - 2 $\mathbf{z}_U^0 \leftarrow \mathbf{0}$ ▷ initial guess
 - 3 $\mathbf{z}_U^{\text{LP}} \leftarrow \text{ConjugateGradient}(\mathcal{L}_{UU}, -\mathcal{L}_{UL} \mathbf{z}_L, \mathbf{z}_U^0)$
-

A.2 Stochastic logdet Estimation with Flux.jl

The base GNN regressors are implemented in Julia with Flux.jl [19]. For better compatibility with the underlying GNN, we implement the stochastic estimation algorithm using the “customized gradient” interface provided by Flux.jl. For example, Listing 1 shows the code snippet that defines the log-determinant computation: when `logdetΓ` is invoked, its output is tracked and its derivative can be computed automatically with back-propagation. This scheme greatly simplifies the downstream implementations for data mining experiments, and it works as if we were computing the exact gradient — only orders of magnitude faster with a minor loss of accuracy, as evidenced by our experiments in Section 3.2.

A.3 Additional Details on Experimental Setup

Neural network architecture. Our regression pipeline first encodes each vertex into a 8-dimension representation using an MLP or GNN and then uses a linear output layer to predict its label. For the MLP, we use a 2-hidden-layer feedforward network with 16 hidden units and ReLU activation function. Each GNN we consider also consists of 2 layers, each with 16 hidden units and ReLU activation function.

```

1 using Flux.Tracker: track, @grad
2
3 # When this function is invoked, Flux automatically
4 # tracks the output for auto-differentiation
5 logdetΓ(α, β; S, t, k) = track(logdetΓ, α, β; S=S, t=t, k=k);
6
7 # This tells Flux how to track logdetΓ
8 @grad function logdetΓ(α, β; S, t, k)
9     """
10     Input:
11     α: (vector of) model parameters
12     β: model parameter
13     S: (vector of) normalized adjacency matrices
14     t: # of trial vectors
15     k: # of Lanczos tridiagonal iterations
16
17     Output:
18     1): logdet(Γ)
19     2): map from sensitivity of logdet(Γ)
20         to sensitivity of α, β
21     """
22     # sample Gaussian random vector
23     n = size(S,1);
24     Z = randn(n,t);
25
26     # eqns (5) in this paper
27     Γ = getΓ(α, β; S=S);
28     ∂Γ∂α = get∂Γ∂α(α, β; S=S);
29     ∂Γ∂β = get∂Γ∂β(α, β; S=S);
30
31     # adopted from Gardner 2018 GPytorch paper
32     X, TT = mBCG(Y->Γ[P,P]*Y, Z; k=k);
33
34     # eqn (20) in this paper
35     vv = 0;
36     for T in TT
37         eigvals, eigvecs = eigen(T);
38         vv += sum(eigvecs[1,:].^2 .* log.(eigvals));
39     end
40     Ω = vv*n/t;
41
42     # eqn (18) in this paper
43     trΓiM(M) = sum(X.*(M[P,P]*Z))/t;
44     ∂Ω∂α = map(trΓiM, ∂Γ∂α);
45     ∂Ω∂β = trΓiM(∂Γ∂β);
46
47     return Ω, Δ -> (Δ*∂Ω∂α, Δ*∂Ω∂β);
48 end

```

Listing 1: Code snippet for estimating the log-determinant and its derivatives.

Optimization. For all but the Twitch-PT datasets, the framework parameters α, β are optimized using gradient descent with learning rate 10^{-1} . The Twitch-PT dataset uses a limited-memory BFGS optimizer. For the MLP and GNN experiments summarized in Table 1 and Fig. 5, the neural network parameters are optimized for 75 epochs using the Adam optimizer with $\beta_1 = 0.9, \beta_2 = 0.999$, and learning rate 10^{-3} . For the inductive experiments summarized in Fig. 6, the neural network parameters are further fine-tuned for 25 epochs with the Adam optimizer at a smaller learning rate 5×10^{-4} . All of our experiments are performed on a single workstation with an 8-core i7-7700 CPU @ 3.60GHz processor and 32 GB memory.

A.4 Additional Details on Datasets

Ising model simulations. The Ising model simulates on a two-dimensional grid graph. For each vertex i , there is a discrete variable $\sigma_i \in \{-1, +1\}$ representing its spin state. A spin configuration σ assigns a spin state to every vertex in the graph. Ising model considers two type of interactions: (i) interaction between spin of each

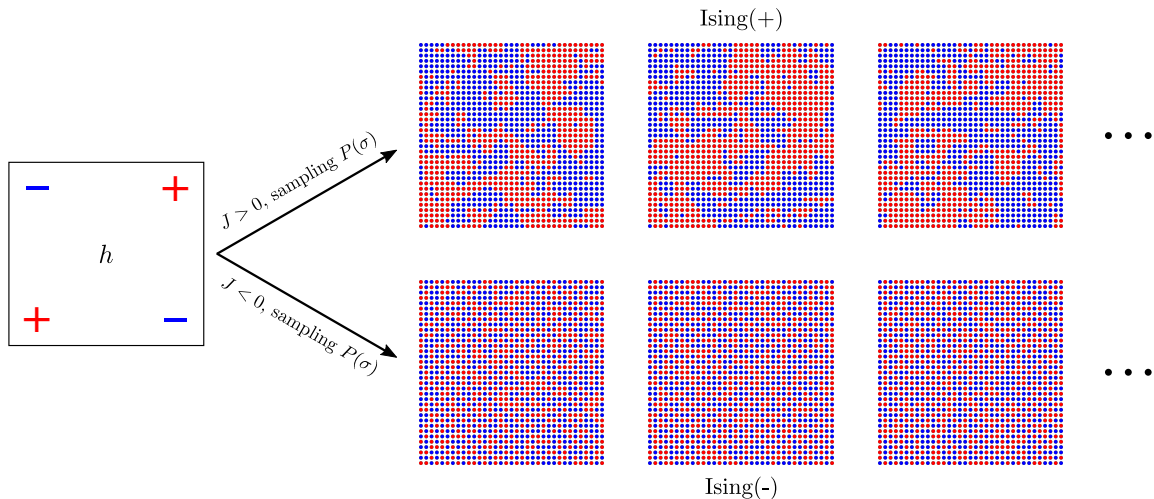


Figure 7: Example Ising spin configurations sampled from the Boltzmann distribution. Vertices with +1 spins are colored in red, and vertices with -1 spin are colored in blue.

Table 2: Transductive learning accuracy of our framework, using different GNN architecture as the base predictor.

Dataset	GCN			GraphSAGE-max			GraphSAGE-polling		
	GNN	LP-GNN	C-GNN	GNN	LP-GNN	C-GNN	GNN	LP-GNN	C-GNN
Ising(+)	0.61 ± 0.04	0.72 ± 0.03	0.72 ± 0.03	0.67 ± 0.04	0.76 ± 0.02	0.76 ± 0.02	0.67 ± 0.04	0.76 ± 0.02	0.76 ± 0.02
Ising(-)	0.47 ± 0.02	0.34 ± 0.02	0.70 ± 0.03	0.47 ± 0.02	0.30 ± 0.03	0.77 ± 0.03	0.48 ± 0.02	0.30 ± 0.03	0.77 ± 0.02
income	0.60 ± 0.04	0.61 ± 0.05	0.62 ± 0.04	0.73 ± 0.03	0.79 ± 0.03	0.78 ± 0.04	0.74 ± 0.03	0.78 ± 0.03	0.77 ± 0.02
education	0.45 ± 0.04	0.44 ± 0.04	0.47 ± 0.04	0.67 ± 0.02	0.70 ± 0.02	0.70 ± 0.03	0.68 ± 0.02	0.70 ± 0.03	0.70 ± 0.03
unemployment	0.49 ± 0.03	0.72 ± 0.03	0.72 ± 0.03	0.57 ± 0.05	0.74 ± 0.04	0.75 ± 0.05	0.60 ± 0.05	0.74 ± 0.04	0.75 ± 0.04
election	0.45 ± 0.03	0.61 ± 0.02	0.60 ± 0.02	0.43 ± 0.04	0.64 ± 0.03	0.65 ± 0.03	0.49 ± 0.06	0.66 ± 0.02	0.65 ± 0.02
Anaheim	0.69 ± 0.05	0.75 ± 0.05	0.75 ± 0.05	0.73 ± 0.04	0.79 ± 0.05	0.80 ± 0.04	0.74 ± 0.04	0.80 ± 0.04	0.80 ± 0.05
Chicago	0.58 ± 0.05	0.63 ± 0.05	0.63 ± 0.05	0.64 ± 0.05	0.68 ± 0.05	0.68 ± 0.05	0.66 ± 0.05	0.69 ± 0.04	0.68 ± 0.04
sexual	0.77 ± 0.04	0.72 ± 0.04	0.92 ± 0.02	0.86 ± 0.02	0.86 ± 0.02	0.92 ± 0.02	0.85 ± 0.05	0.85 ± 0.04	0.92 ± 0.02
Twitch-PT	0.54 ± 0.02	0.65 ± 0.01	0.64 ± 0.02	0.69 ± 0.04	0.69 ± 0.04	0.70 ± 0.03	0.72 ± 0.03	0.72 ± 0.03	0.71 ± 0.03

vertex with external field and (ii) interaction between neighboring spins. Those interactions constitute the “energy” for each spin configuration:

$$H(\sigma) = - \sum_{(i,j) \in E} J_{ij} \sigma_i \sigma_j - \sum_{i \in V} h_i \sigma_i, \quad (24)$$

where J_{ij} controls the interaction between neighboring vertices, and h_i denotes the external field on vertex i . Finally, the configuration probability is given by the Boltzmann distribution,

$$P(\sigma) = \frac{e^{-H(\sigma)}}{\sum_{\sigma'} e^{-H(\sigma')}}. \quad (25)$$

Our Ising spin simulation randomly draws from this Boltzmann distribution. For the Ising(+) dataset, we set $J_{ij} = J = 0.1$ and $h_i = 0.35 \cdot (x_i)_1 \cdot (x_i)_2$, where \mathbf{x}_i is the coordinate of vertex i normalized between -1.0 and $+1.0$. In other words, the physical system favors parallel spins between neighboring vertices, and the external field exhibits “XNOR” spatial pattern. For the Ising(-) dataset, a similar setting is used, except that $J_{ij} = J = -0.1$. Some sampled Ising spin configurations are shown in Fig. 7.

Sexual interaction dataset. The dataset used to construct the sexual interaction network was collected by Colorado Springs project 90, which details the relationships of 7674 individuals. We take the largest connected component in the derived sexual relation network, which consists of 1888 vertices and 2096 edges. Of the 2096 relationships, 2007 are heterosexual and 89 are homosexual.

A.5 Other GNN Base Predictors

We tested a variety of GNN architectures as base regressors in our framework, and Table 2 summarizes the results. Here, we see the exact same trend as describe in Section 4.2: C-GNN greatly improve over GNN on almost all datasets, and LP-GNN outperforms GNN on datasets where vertex labels are positively correlated. These experiments support our claim that the performance gain we observe from exploiting label correlation is robust to change of the underlying GNN architecture.